INDUSTRIAL APPLICATION OF OPEN PORE CERAMIC FOAM FOR MOLTEN METAL FILTRATION

L.J. Gauckler and M.M. Waeber
Swiss Aluminium Ltd.
Research & Development
8212 Neuhausen
Switzerland

C. Conti and M. Jacob-Dulière
Faculté Polytechnique de Mons
7000 Mons
Belgium

Summary

Ceramic foam filters were used for industrial filtration of aluminum. Results are compared with laboratory experiments which are in good agreement with trajectory analyses of deep bed filtration for the early stage of filtration.

The correlations between structural characteristics of the filter media, filtration parameters and filter efficiency are given. In addition the most important parameters for the industrial use of filters are discussed.

Introduction

The increasing use of aluminum alloys for sophisticated products like beverage cans or aircraft components requires extremely low impurity concentrations in the liquid metal. Solid impurities of a few microns may be detrimental for high quality surface finish and products with high deformation rates and small cross sections. Therefore efficient melt purification methods are needed to meet today's high quality standards especially regarding the increasing use of secondary aluminum.

Our objective is to describe the already widely used filtration through open pore ceramic foam filters using a kinetic filtration model. The model predicts filtration efficiency for different filter types and the most important filtration parameters. These data are compared with results from laboratory filtration experiments as well as results from filtration under cast house conditions.

Solid Impurities in Aluminum

A survey of solid inclusions occurring in aluminum is given in Table I (1, 2). The most common solid impurities are globular oxides in magnesium containing alloys and oxide skins.

Table I. Inclusions in Aluminum

	Type	Form	Density (g/cm^3)	Dimensions (μm)
OXIDES	Al_2O_3	Particles Skins	3.97	0.2 - 30 10 - 5000
	MgO	Particles Skins	3.58	0.1 - 5 10 - 5000
	$MgAl_2O_4$	Particles Skins	3.6	0.1 - 5 10 - 5000
	SiO_2	Particles	2.66	0.5 - 5
NON OXIDES	Salts Chlorides Fluorides	Particles	1.98 - 2.16	0.1 - 5
	Carbides Al_4C_3 SiC	 Particles Particles	 2.36 3.22	 0.5 - 25
	Nitrides AlN	Particles Skins	3.26	10 - 50
	Borides TiB_2 AlB_2	Particle- Clusters Particles	 4.5 3.19	 1 - 30 0.1 - 3

The observed particle size in aluminum melts varies between inclusion dispersoids of a few microns to oxide skins of several milimeters.

Molten Metal Cleaning Methods

There are various methods available to remove impurities from metal melts. Some of them are listed in Table II. They are based on sedimentation, flotation or filtration. A good survey of the fundamentals of molten aluminum filtration can be found in reference 3.

Table II. Melt Cleaning Methods

Method	Impurities removed	Type
Sedimentation	particles, skins	furnace treatment
Flotation	particles, skins hydrogen, alkali- trace elements non-metallic inclusions	- furnace treatment - "SNIF" - "MINT" - "DUFI" - "FILD"
Filtration sieving deep bed filtration cake filtration	particles, skins " " " "	- woven cloth filter - SELEE ceramic foam - Alcoa 469 ball bed filter - FILD (ceramic spheres) - Metaullics (ceramic tubes)

Sedimentation is performed by long time furnace treatment. Flotation is done in separate treatment units similar to small holding furnaces of several tons capacity. The units in general are supplied with a heating system. An exception is the system MINT with its small volume which can be emptied after each cast. Some of the units filtering solid particles are used for single drop application, like ceramic foam filters.

The intent of this paper is to describe the filtration of aluminium using ceramic foam filters.

Filtration

Particles are removed in the filtration process by the filter medium in three different ways depending on size of the particles and size of the openings in the filter medium.

Sieving takes place on the surface of the filter medium forming a filter cake in the case of particle diameters which are of the same order of size or larger than the holes in the filter medium (Figure 1). Woven cloth filters are mainly operating in this mode.

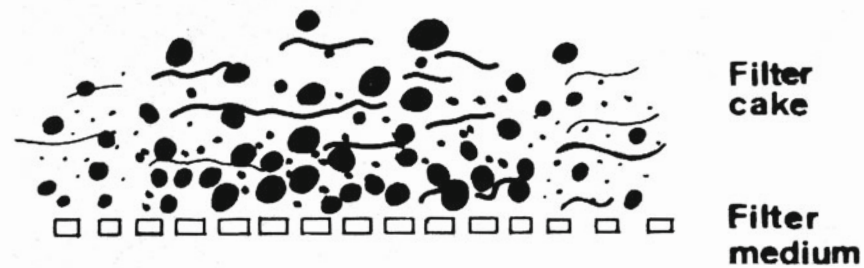

Figure 1 - Sieving and cake filtration
skins particles

Deep bed filtration occurs within the granular or foamed filter medium on its internal surface. Each internal pore surface has a probability of retaining particles from the melt (Figure 2). In this case, particles are smaller than the smallest opening, the "window size".

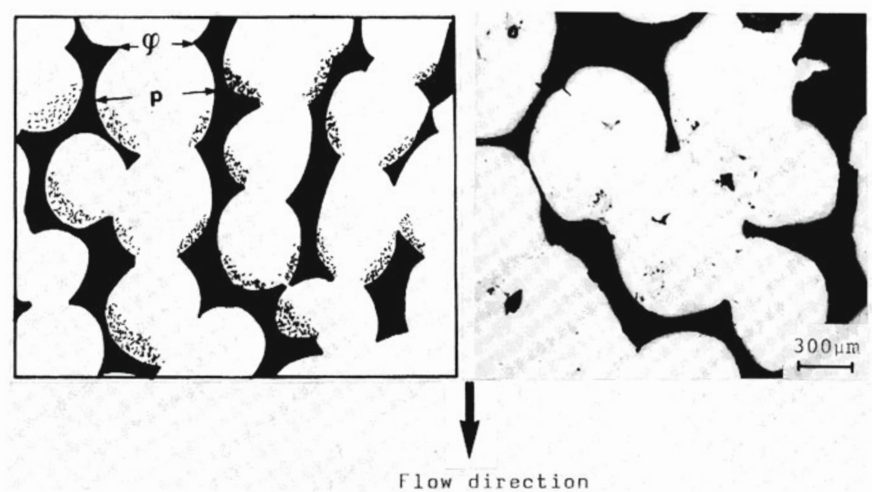

Figure 2 - Deep bed filtration (two dimensional cuts of a ceramic foam, left image schematically)
ϕ = window size p = cell size

Impurity particles can be detected after filtration inside the filter structure near the internal surface of the filter media.

Transport Mechanisms

There are several reasons for a particle to touch the internal macroscopic surface of the filter. The following transport mechanisms shown in Figure 3, were taken into account by Conti (2) to calculate filter efficiencies for aluminum filtration.

Direct interception. A particle hits the filter surface following its trajectory line.

Gravity forces. A particle with specific density different from the fluid leaves the trajectory line caused by gravity forces.

Brownian movement. Is the microscopic movement caused by the molecular bombardment on the particles in the liquid. This phenomena is believed to be important only for submicron particles.

Inertial forces. Caused by the apparent weight of the particle which cannot follow sudden changes of the trajectory line and hits the internal filter surface.

Hydrodynamic effects. They are due to the velocity distribution in the filter cell. Depending on the shape of the particle it rotates and translates in the flow field.

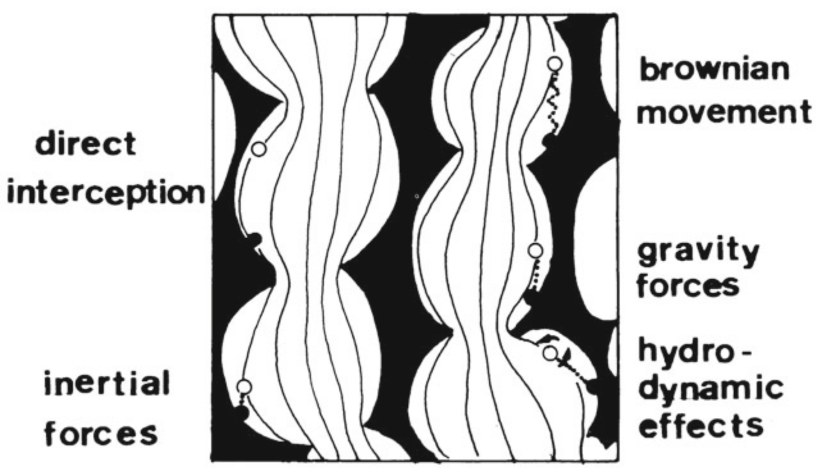

Figure 3 - Tranpsort mechanisms of a particle in deep bed filtration.
—— trajectory line

In the case of aluminum filtration with ceramic foam the most important forces are direct interception, inertial and hydrodynamic forces.

In the case of a particle which has touched the internal filter surface it is attached by Van der Waals forces. Particles, or aggregates of particles may be detached from the filter surface by increasing shear stresses. They are caused by a sudden increase of flow rate, by backwashing or pumping mode of the flow as well as by sudden movement of the filter media itself.

Structure of Open Pore Ceramic Foam

Information about the structure of the filter medium is basic to understand fluid flow characteristics. Stereological methods (4) were used to characterize the microstructures of the ceramic foams. Micrographs of a cross-section and of the two-dimensional ceramographic sample of a three-dimensional foam are shown in Figure 4.

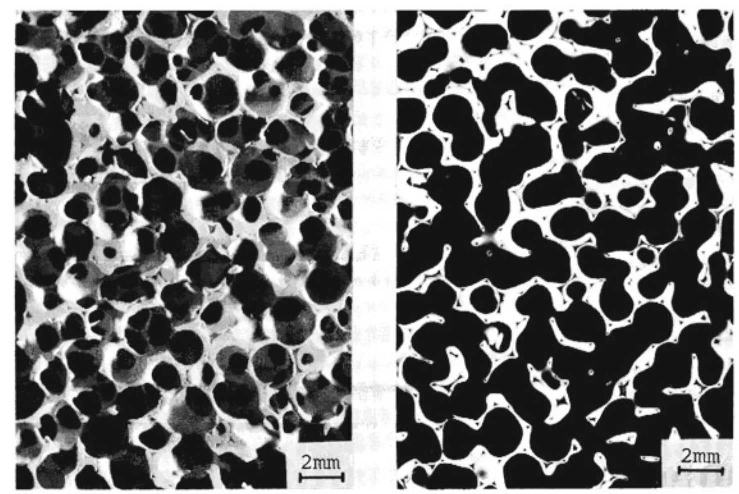

Figure 4 - Three- and two-dimensional images of the ceramic foam.

The three-dimensional structure can be analysed by lineal analysis (4) of the two-dimensional micrograph. Definitions and relations of the measured features are given in Table I of the appendix.

The most important stereological parameters to describe the ceramic foam structure are shown in Figure 5.

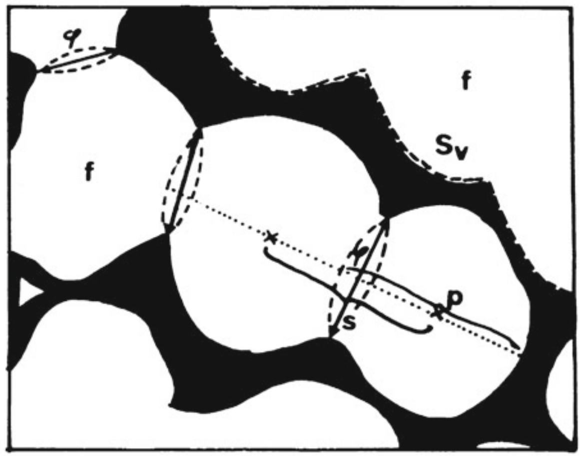

Figure 5 - Stereological parameters of the ceramic foam.

The structure of the ceramic foam consists of rounded polyhedra (5) with diameter p which are connected to each other by openings (windows) of diameter ϕ . A rough characterization is given by the number of pores per inch (ppi). The total porosity is designated f, the total internal cell surface S_V. The distance of the centers of two cells is s. The interrelation between these foam parameters and the lineal analysis parameters are given in Table II of the appendix. In Table III the results of the stereological analysis of different filters ranging from 55 to 24 ppi are shown.

Table III. Ceramic Foam Filter Spacing Parameters

Filter type	Macro-porosity f (%)	Mean window size $\bar{\phi}$ (mm)	Mean cell size $\bar{p}$ (mm)	Mean cell size $\bar{p}_1$ (mm)	Internal surface S_V (m^2/m^3)
55 ppi	81±1	0.60±0.1	0.91±0.2	1.10±0.1	3.85±0.4
40 ppi	81±1	0.85±0.1	1.37±0.2	1.56±0.2	3.12±0.2
30 ppi	75±2	1.0±0.05	1.81±0.15	2.20±0.2	2.25±0.3
24 ppi	63±2	1.45±0.3	2.20±0.4	-	1.50±0.4

The ceramic foam structure shows anisotropy. In the plane of the filter plate, the cells are spherical with a mean cell size of $\bar{p}$. Perpendicular to the filter plate, the cells are elongated with a somewhat larger mean cell size of $\bar{p}_1$.

Open Macroporosity, Cell and Window Size

In ceramic foam filters the determining dimensions for permeability and fluid flow are the mean cell and window size. Figure 6 shows the relation between these two parameters.

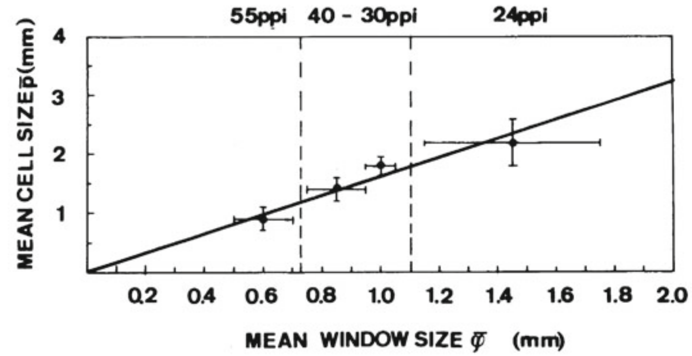

Figure 6 - Relation between cell and window size.

From 55 to 24 ppi the values of the mean cell size perpendicular to the flow direction increases from 0.9 to 2.2 mm and the mean window size increases from 0.6 to 1.45 mm. The total open macroporosity of the ceramic foam ranges from 75 % (30 ppi) to 83 % (24 ppi).

Internal Surface

This is the surface which is in contact with molten metal during filtration. Due to the surface tension of the molten metal, pores smaller than approximately 0.1 mm can hardly contribute to this internal surface for metal pressures usually applied in filtration do not exceed 500 to 1000 mm Al metallostatic pressure. In Figure 7 the internal surface as a function of the mean window size is shown. It decreases from 4.0 to 1.0 m^2/m^3 for 55 to 24 ppi filters.

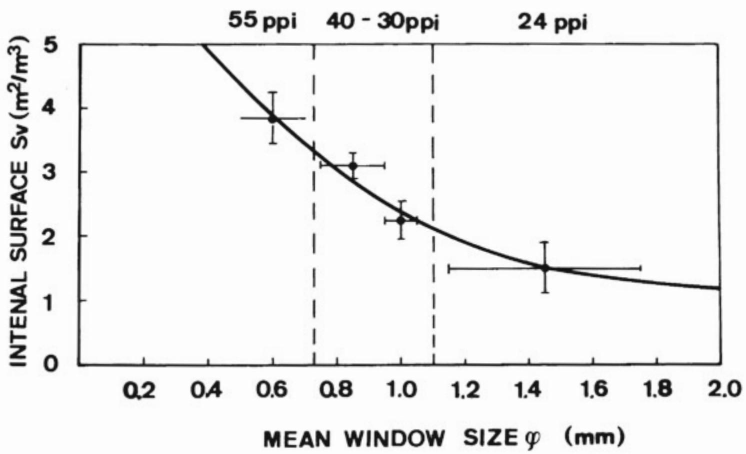

Figure 7 - Macroscopic internal surface of ceramic foam filters.

Trajectory Model

Initial filter efficiencies were calculated by Conti (2), Jacob and Conti (6) using Payatakes, Tien and Turian's method of trajectory calculations (7, 8). This method is well established and successfully employed for water and aerosol filtration.

The efficiency of deep bed filtration is:

$$\eta = \eta_c \cdot p \qquad (1)$$

where η_c = the probability of contact between particles and internal filter surface

and p = retention probability of a particle in contact with the internal surface.

In this study, the probability of retention after contact is taken to 1 ($p = 1$). Therefore the filter efficiency is determined by the probability of the particles to contact the internal surface of the filter.

According to the periodicity of the unit cells in the flow direction, the filtration bed can be divided into a series of identical unit elements with height H_{cell} which is equal to the periodicity (Figure 8). It is assumed that the concentration of particles at the beginning of each cell is uniform perpendicular to the flow.

Thus it is possible to calculate the probability of particle attachment (η_c) by distinguishing particles on trajectory lines collisioning with the cell-surface from particles which simply pass trough the cell.

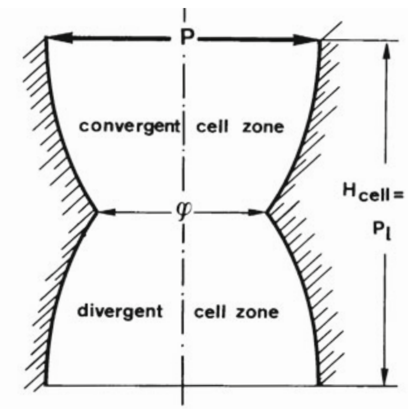

Figure 8 - Model of dimensionless unit cell after Conti (2).

The retention probability of a unit cell is given by λ_o, the filtration coefficient:

$$\lambda_o = \frac{1}{H_{cell}} \ln\left(\frac{1}{1 - \eta_c}\right) \qquad (2)$$

The filter efficiency of a filter with thickness H is:

$$\eta = \frac{c_{in} - c_{out}}{c_{in}} = 1 - e^{-\lambda_o \cdot H} \qquad (3)$$

where c_{in} = inlet concentration of particles
c_{out} = outlet concentration of particles.

The calculation of the trajectory lines along which inclusions follow in suspension requires solution of the Navier-Stokes equations, either by an analytical approach or by the method of calculating finite differences in the velocity field.

Figure 9 shows the trajectory lines for different Reynolds numbers (equal to different melt velocities) in a unit cell of the filter.

The Reynolds number is defined by:

$$Re = \frac{v_o \cdot H_{cell}}{\nu} \qquad (4)$$

where ν = viscosity of aluminum (0.0059 cm^2/s)
v_o = velocity of aluminum in the smallest cross section of the structure

$$v_o = \frac{v_s}{N_p \cdot \pi \cdot (\phi/2)^2} \qquad (5)$$

where v_s = apparent macroscopic melt velocity through the porous structure
N_p = number of unit cells per filter thickness.

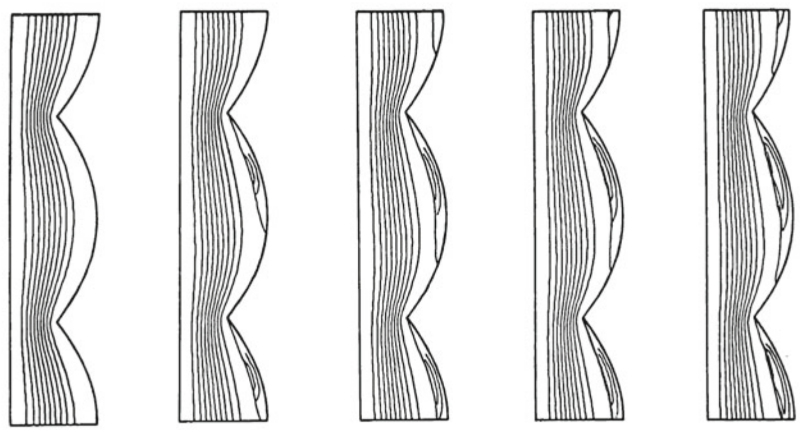

Figure 9 - Calculated trajectory lines for different Reynolds numbers.

The main portion of attachment occurs in the convergent zone of the cell. In the divergent zone, the trajectory lines deform at high Reynolds numbers. Therefore the probability of attachment in this area is lower.

Calculated Filter Efficiencies

The following figures illustrate the filter efficiencies for 2 inch thick filter plates as a function of :

- filter type: 55, 40, 30 ppi
- melt velocity: v_s = 0.2 ... 1.6 cm/s
- particle dimension: d_p = 1 ... 50 µm
- particle specific gravity: ρ_p = 2.36... 4.5 g/cm^3

Filter Efficiency as a Function of Melt Velocity.

The filter efficiencies range from 75 to 95 % for 20 µm particles at low melt velocities and decrease to the range of 15 to 35% for high melt velocities and small particles as shown in Figure 10.

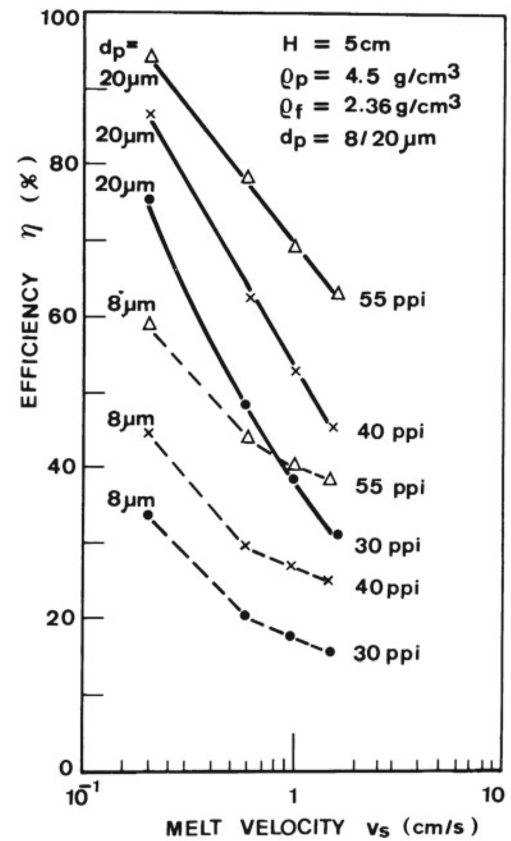

Figure 10 - Calculated initial filter efficiencies as a function of melt velocity.

Decreasing efficiency with increasing melt velocity is due to the increased turbulence in the convergent zone of the pores, and the diminished sedimentation possibility at higher melt velocities.

Filter Efficiency as a Function of Particle Dimension.

Filter efficiency is increasing with increasing particle size. In Figure 11 examples are shown for particles with densities of 4.5 g/cm^3 and melt velocity of 1.0 cm/s. More than 80 % of all particles greater than 40 µm are removed from the melt. Even for particles of 20 µm diameter, efficiencies were obtained ranging from 30 to 65 % for finer filter (55 ppi) (2, 6).

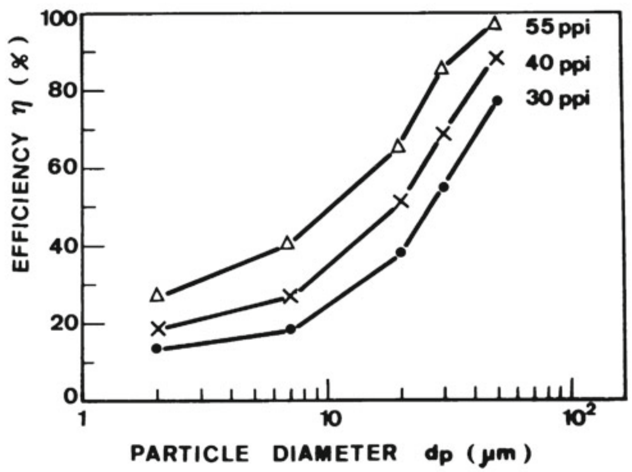

Figure 11 - Calculated initial filter efficiencies as a function of particle dimension.
$H = 5$ cm, $\rho_p = 4.5$ g/cm^3, $\rho_f = 2.36$ g/cm^3
$v_s = 1.0$ cm/s.

Filter Efficiency as a Function of the Particle's Specific Gravity.

If the particles are heavier than the liquid, the effect of sedimentation becomes more important. In consequence the particle retention in the convergent part of the cell is favorised. This is illustrated in Figure 12. Efficiency is increasing with increasing specific gravity of the particles. This behaviour is more pronounced for coarse filters (30 ppi) than for fine filters (55 ppi).

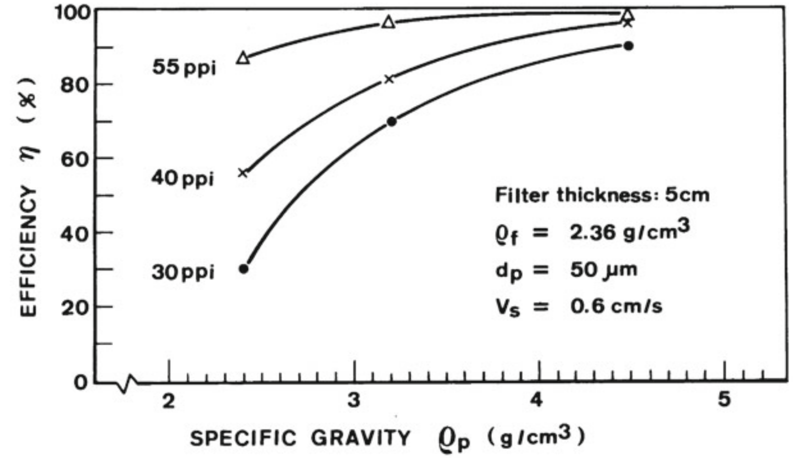

Figure 12 - Calculated initial filter efficiencies as a funtion of the particle's specific gravity.

Laboratory Experiments

The initial filter efficiencies of different filter types were experimentally proven using titanium diboride particles as tracers in aluminum melt. The experimental arrangement used for these experiments is shown in Figure 13.

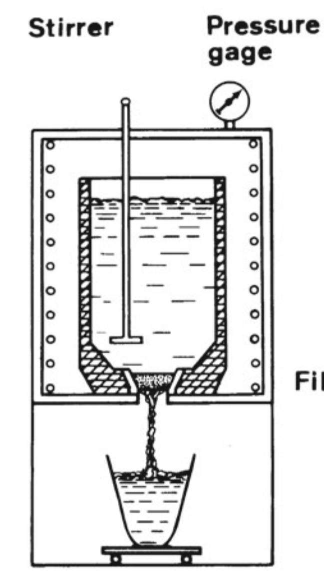

Figure 13 - Experimental apparatus.

The filter is placed in the bottom of a cast iron crucible inside a resistance furnace. Aluminum of 99.85 % purity with titanium diboride from Kawecki Berylco (master alloy Al-Ti5%/B1%) were used. The TiB_2 particles range from 1 to 10 μm in diameter. The concentration is detected by spectrographic techniques using boron and titanium signals.

For each run an amount of about 4 to 9 kg aluminium melt with different quantities of master alloy from 2 to 5.4 weight-% is heated up to at least 720°C. The melt is agitated by 2oo revs./min during 15 min. This ensures a homogenous melt. Experiments with 30 and 40 ppi were performed by Conti (2). The compositional range of the melt is between 0.1 to 0.27 % Ti and 0.02 to 0.054 % B. Flow rates during filtration are recorded by an electronic balance underneath the second crucible.

Samples of the melt before and after the filter were collected at regular time intervals for spectrographic analysis. This allows determination of the efficiency η of a filter medium according to:

$$\eta = \frac{(TiB_2)_{in} - (TiB_2)_{out}}{(TiB_2)_{in}} \qquad (3)$$

Three analyses were used in each run to determine the ingoing and outgoing tracer concentration. The average values were used to calculate the filter efficiency η for 2 inch filters according to equation 3. Typical experimental results of 55 ppi filters are listed in Table III of the appendix. Detailed results of single runs for 40 and 30 ppi filters can be found in reference (2).

In Figure 14, the filter efficiencies are given as a function of melt velocity. The results from laboratory experiments are represented by the shaded areas. Dotted lines are the calculated efficiencies for 8 μm TiB_2 particles. The experimental results are in good agreement with the calculated values. Efficiencies increase for decreasing melt velocities. Efficiencies are higher for finer filters (55 ppi) with high internal surface and lower for coarser filters (30 ppi).

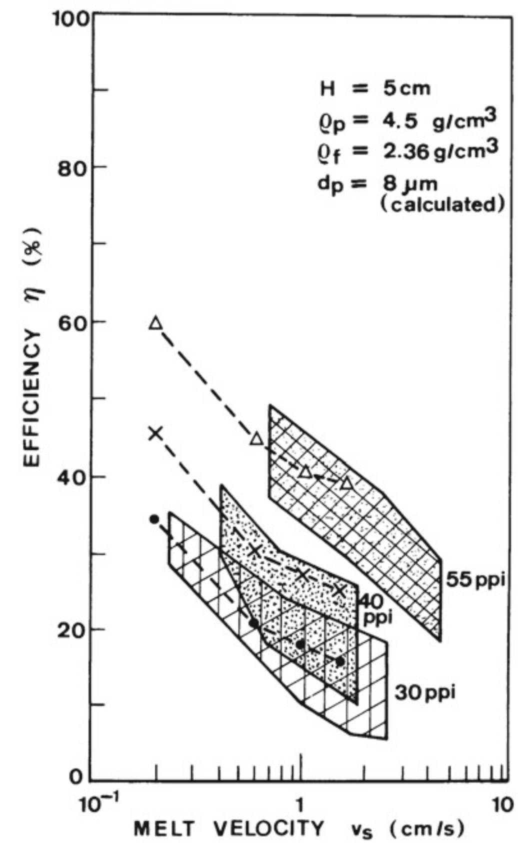

Figure 14 - Experimental and calculated (dotted lines) efficiencies of ceramic foam filters for different melt velocities.

Aluminium Cast House Experience

In the following the working parameters and efficiencies of ceramic foam filters in industrial application are discussed.

Ceramic filters are best used in-line between furnace and casting machine (Figure 15). Filters are preheated prior to casting. The metal level difference Δh is used as the driving force to obtain fluid flow through the filter.

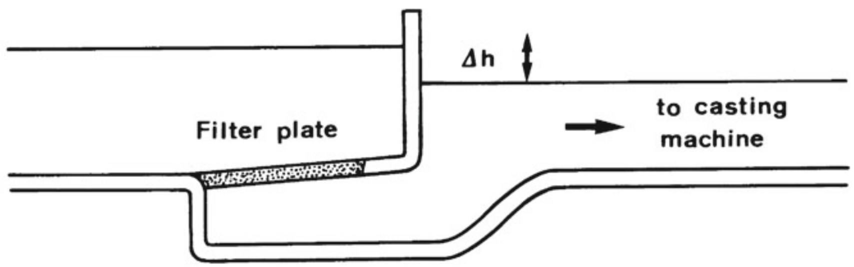

Figure 15 - Industrial in-line application of ceramic foam filters.

Constant Rate Filtration

Prior to filtration the filter has to be impregnated with aluminum by a metal pressure h_p higher than that used during filtration. This is illustrated in Figure 16 showing metal pressure on the filter for constant rate filtration.

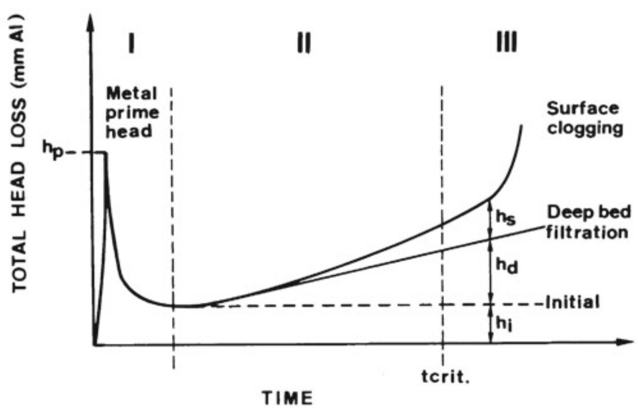

Figure 16 - Total head loss varying with time during constant rate filtration.

After impregnation has taken place, the head loss h_i is the metal level difference between ingoing and outgoing metal which is needed for a constant flow through the porous medium.

During constant rate filtration the increase of metal level increases by the difference Δh per time Δt according to the deposition of impurities on, or in the filter plate (9). This metal level difference increases almost linearly with time during phase II of filtration. During this phase II impurities deposit inside the filter mainly, but also on the filter forming a filter cake which is compressed in phase III. Then the filter clogs and the metal level difference Δh increases drastically with time. At the beginning of phase III metal filtration should be terminated.

Metal prime head h_p. For different filter types the metal prime head h_p is given in Figure 17.

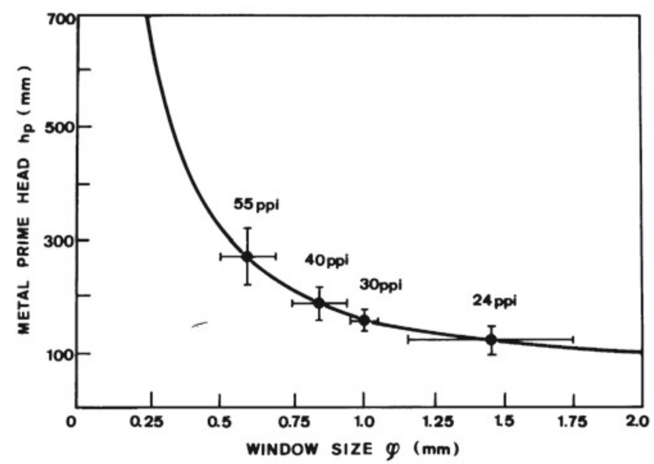

Figure 17 - Metal prime head for different filters versus window size.

Metal prime head is mainly determined by the window size of the filters. It can be expressed by:

$$p = - \rho \cdot g \cdot h_p = \frac{4 \cdot \gamma_{LS}}{\phi} \cos\theta \qquad (6)$$

where p is the pressure, ρ the density of the melt (2.4 g/cm^3), h_p the metal prime head in mm, γ_{LS} the surface energy solid/liquid (Al_2O_3/Al = 860 dyn/cm) and θ the wetting angle of aluminum on alumina (≈ 176°).

Using these values, the metal prime head is expressed by:

$$h_p \text{ (mm)} = 146 \text{ (mm}^2\text{)} \quad \frac{1}{\phi \text{ (mm)}} \qquad (7)$$

Calculated and experimental values are in good agreement.

Working Metal Head h_d. At the beginning of filtration after impregnation, the working metal head is determined by the specific flow resistance of the filter, the filter size and the flow rate. Recommended flow rates and filter types are given in Figure 18. Working metal heads for the recommended range are typically 5 to 50 mm.

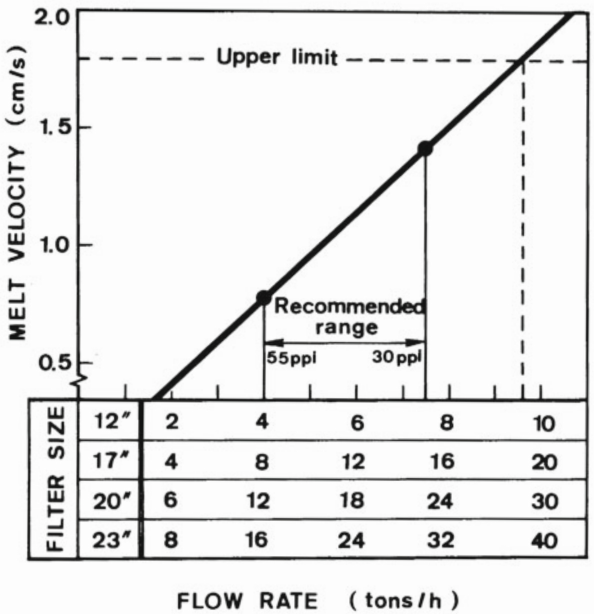

Figure 18 - Flow rates for different ceramic foam filters.

Besides the mentioned parameters, the impurity level of the first metal approaching the filter determines working metal level also. Precleaning of this first metal by removing large oxide skins avoids clogging of filter surface. This results in low working metal heads and extended filter lifetime can be expected.

Total drop size, e.g. the critical time when the filter starts to clog is determined by the impurity level of the melt. The increase of working metal level versus time can be measured and used to characterize the quality of the melt and the lifetime of the filter.

Filter Efficiency

Filter efficiencies in cast house operation were determined by analysing the type and amount of impurities in chilled metal samples as described in reference (1). Differences of impurity concentrations before and after the filter were used for efficiency characterization as shown in Figure 19.

SELEE 30 ppi; 17"	Alloy 6110 (Al-Mg-Si)	
Total number of probes	: (A) 27	(B) 27
Total number of inclusions	: (A) 80	(B) 23
Average size of inclusions (µm)	: (A) 135	(B) 119
EFFICIENCY	:	η = 71.3 %

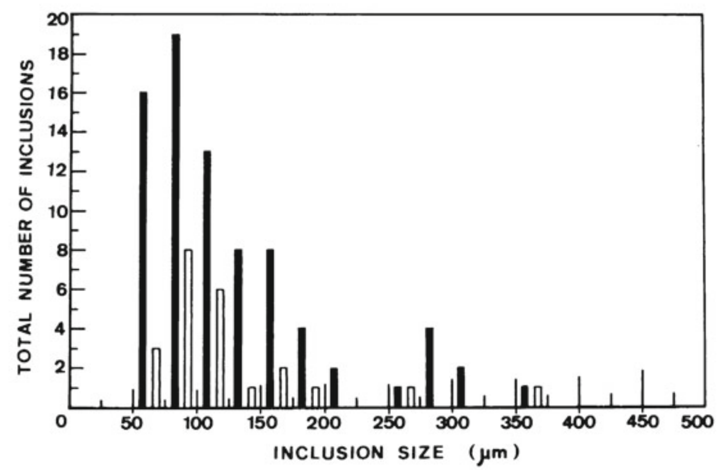

Figure 19 - Size distribution of inclusions (A) before ▬ (B) after ▭ filter.

The data in Figure 19 are based on 54 specimens of 100 cm^2 each from 10 different casts using flow rates of 13 tons/h and drop size of 21 tons. Inclusions smaller than 20 µm were not counted. Total number of inclusions taken in specimens before the filter were 80, after the filter 23. About 80 % of the inclusions were identified as oxide particles and skins. The rest were salts and borides. A total efficiency of 71 % was obtained.

The Table IV summary of results shows the effects of filtration parameters.

Table IV. Filter Efficiency

	Filter efficiency	
	high for	low for
particles	- large - high specific gravity	- small - low specific gravity
filter medium	- large internal surface - small window size (equal to high number of pores per inch)	- small internal surface
liquid flow	- low melt velocity - laminar flow in filter medium - steady flow	- high melt velocity - turbulent flow in filter medium - pumping mode operation

Conclusions

Filter efficiencies of ceramic foam filters calculated for the early stage of filtration using the trajectory model are in good agreement with results of laboratory experiments using TiB_2 particles as tracers. Both indicate the deep bed filtration process to be dominant during the early stage of filtration.

Metal prime head for filtration start up is directly determined by the pore size of the filters. Specific flow rates and type of filter define the metal head loss during constant rate filtration.

Filter efficiencies under cast house conditions were found to be almost 100 % for oxide inclusions larger than 100 µm for a 30 ppi filter. An average filtration efficiency of almost 80 % was observed for high Mg-containing alloys.

References

1. K. Buxmann, P. Furrer, "Zum Problem der grauen Zeilen auf anodisch oxidierten Aluminiumprodukten", Metall, 34 (3) (1980) pp. 222 - 228.
2. C. Conti, "Contribution à l'étude de la filtration profonde des métaux", Thesis, Faculté polytechnique de l'Université de Mons, Belgium, 1983.
3. C.E. Eckert, R.E. Miller, D. Apelian and R. Mutharasan: "Molten Aluminum Filtration: Fundamentals and Models", pp. 1281 - 1304 in Light Metals 1984, J.P. McGeer, ed.; Conference Proceedings, The Metallurgical Society of AIME.
4. E.E. Underwood, "Quantitative Stereology", p. 274, Addison-Wesley, Massachusetts, USA, 1970.
5. J.R. Dawson, J.B. Shortall, "The microstructure of rigid polyurethane foams", Journal of Material Science, 17 (1982) pp. 220 - 224.
6. M. Jacob, C. Conti, "Etude des probabilités initiales d'arrêt d'inclusions dans des filtres pour métaux", Internal report, Alusuisse Research & Development, Neuhausen, Switzerland; Faculté polytechnique de Mons, Belgium, 1984.
7. A.C. Payatakes, C. Tien, R.M. Turian, "A New Model for Granular Porous Media", A.I.Ch.E. Journal, 19 (1) (1973) pp. 58 - 76.
8. A.C. Payatakes, C. Tien, R.M. Turian, "Trajectory Calculation of Particle Deposition in Deep Bed Filtration", A.I.Ch.E. Journal, 20 (5) (1974) pp. 889 - 905.
9. K.J. Ives, "Deep Bed Filtration", pp. 284 - 301 in Solid-Liquid Separation, L. Savarovsky, ed., Butterworths, London, 1981.

Appendix

Table I. Basic Symbols used in Microstructure Analyses and their Definitions after Underwood (4)

Definition	Symbol	Dimension
Lenght of lineal elements or test line length.	L	mm
Lineal fraction. Length of lineal intercepts of cells per unit length of test line.	L_L	mm/mm
Lineal fraction. Length of lineal intercepts of ceramic rods per unit length of test line.	L_C	mm/mm
Number of features.	N	
Number of interceptions of features per unit length of test line.	N_L	mm^{-1}
Average lineal intercept, L_L / N_L.	$\bar{L}$	mm
Internal surface per unit test volume.	S_V	mm^2/mm^3

Table II. Parameters for Ceramic Foam Characterization

Definition	Symbol	Dimension	Formula
Macroporosity	f	%	$\frac{L - L_c}{L} . 100$
Mean cell size	$\bar{p}$	mm	$\bar{L} = \frac{L_L}{N_L}$ $\bar{p} = 3/2\ \bar{L}$
Mean spacing between cells	$\bar{s}$	mm	$\frac{L}{N_L}$
Mean window size	$\bar{\phi}$	mm	$h = \frac{s}{2}$
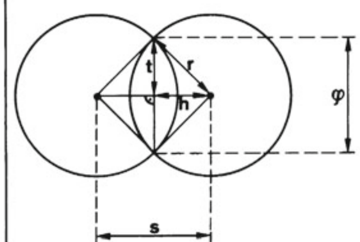			$t^2 = r^2 - h^2$ $t^2 = r^2 - \frac{s^2}{4}$ $t = \sqrt{r^2 - \frac{s^2}{4}}$ $\phi = 2\ t$
Internal surface	S_v	m^2/m^3	$4 \frac{L}{N_L}$

Table III. Experimental Results of 55 ppi Filters

v_s (cm/s)	$(TiB_2)_{in}$ (%)	$(TiB_2)_{out}$ (%)	η H = 2.5 cm (%)	λ_o (cm^{-1})	η H = 5 cm (%)
0.7	0.151	0.113	25.2	0.1161	44.0
0.8	0.153	0.121	20.9	0.0939	37.7
0.9	0.155	0.113	27.1	0.1264	46.8
1.2	0.135	0.106	21.5	0.0968	38.4
1.5	0.161	0.132	18.0	0.0794	32.8
2.0	0.139	0.117	15.8	0.0688	29.1
2.0	0.177	0.138	22.0	0.0994	39.2
2.2	0.152	0.125	17.8	0.0784	32.4
2.5	0.149	0.127	14.8	0.0641	27.4
3.0	0.177	0.155	12.4	0.0530	23.3
3.4	0.167	0.145	13.2	0.0566	24.6
4.0	0.209	0.187	10.5	0.0444	19.9